

# RUBBER/FOAM/COMPOSITE OVERLAY ONTO GUIDE B OF BARRIER LOCATED ON ROAD BEND

MARIAN KLASZTORNY<sup>1</sup>, DANIEL B. NYCZ<sup>2</sup>, ROMAN K. ROMANOWSKI<sup>3</sup>

Military University of Technology, State Vocational Academy in Sanok, ROMA Co. Ltd.

## Summary

The paper examines the SP-05/2 outer barrier of the N2-W4-A class (the producer: Stalprodukt JSC, Bochnia) with the B-type guide bar, located on a horizontal arch to an accelerated traffic main road (Polish code: GP), with the allowable radius of the road axis belonging to the range of 140–220 m. In order to ensure accepting the TB11 crash test, a rubber/foam/composite overlay has been designed, which was combined with the B guide bar with screw connectors using only the empty holes in the guide axis, at 2.00 m intervals. The overlay is flame retardant, resistant to weathering and required chemical effects, increases flexibility and strength of the barrier, reduces vehicle–barrier friction, and its estimated durability is 30 years.

The study develops a method for numerical modelling and simulation of the unmodified (a straight barrier) and modified (a barrier in a horizontal concave arch) TB11 crash test, without and with the overlay, including deformable joints with limited load capacity, contact with friction, tire pressure, posts embedded in deformable subsoil, gravity load, damping, et al.

TB11 virtual crash tests have been conducted for the four above-mentioned barrier design systems. The Geo Metro (Suzuki Swift) car model, corrected respectively, has been taken from the public library developed by the National Crash Analysis Center, USA. Crash tests were simulated using the non-linear explicit finite element code LS-Dyna v971. The results include all the collision parameters required by the EN 1317 standard. It has been proved that the SP-05/2 barrier with the overlay, located on GP road bends, provides acceptance of the TB11 crash test.

**Keywords:** curved road barrier, horizontal concave arch, rubber/foam/composite overlay, TB11 crash test, modelling, simulation

## 1. Introduction

Standards [10, 11] define crash tests and protection parameters in reference to rectilinear road safety barriers. In the case of vehicle collision with a barrier located on a horizontal

<sup>1</sup> Military University of Technology, Faculty of Mechanical Engineering, Department of Mechanics and Applied Computer Science, ul. Kaliskiego 2, 00-908 Warsaw, e-mail: m.klasztorny@gmail.com, tel. 48 22 683 99 47

<sup>2</sup> State Vocational Academy, ul. Mickiewicza 21, 38-500 Sanok, e-mail: daniel.nycz@interia.pl

<sup>3</sup> ROMA Co. Ltd., ul. Słoneczna 7, Grabowiec, 87-124 Złotonia, e-mail: rromanowski@roma.torun.pl

road bend, the vehicle may skid (rotation of car rear), increase the working width, or even stop in the barrier. It is appropriate, therefore, to develop virtual and experimental studies towards verification of the above thesis, as well as towards modification of barriers to accept the required crash tests.

Modelling and experimental verification of road crash tests is the subject of a number of papers. Reference [25] considers a straight road barrier with guide A, wherein easily deformable spacers connecting the guide with posts are applied. The modelling assumes that the guide is a continuous beam without connectors. The elastic-plastic model for steel is adopted. In order to validate the modelling, the numerical results (the ASI index and working width) corresponding to the TB11 crash test [11] were compared with the experimental results.

Reference [4] develops modelling and simulation of TB11 and TB42 crash tests defined in standard [11]. Vehicle models have been taken from the public library of the National Crash Analysis Center (NCAC), USA [31]; a few modifications were made on them. Parts of straight barrier were modelled using shell elements, and bolts were modelled by means of beam or spot-weld elements [12]. The subsoil was reflected using sets of elastic-damping elements. The guiderail was treated as a continuous beam. The influence of four structural changes in the road barrier on its dynamic response was investigated, i.e.:

1) introducing a tension belt, 2) introducing a roll guide, 3) introducing a rope in the upper part of the guide bar, 4) introducing a rope in the lower part of the guide bar. The virtual tests were compared with the full-scale experimental crash tests. The ASI, THIV and PHD parameters were analysed for the TB11 test and the  $W$  working width for the TB42 test.

In Ref. [8], finite element (FE) numerical modelling and simulation of the TB11 crash test was developed, performed on a straight section (36.00m long) of the SP-05/4 road barrier (posts spaced by 4.00 m, the producer: Stalprodukt JSC, Bochnia), without or with an energy intensive cap. The numerical model of Geo Metro car was collected from the NCAC public library [31]. The overlay uses energy intensive foam-steel panels, with trapezoidal cross-section, which are riveted to the B guide bar along the top and bottom edges. It is assumed that the posts are fixed in a rigid substrate. The effects of foam pad density on the energy absorbed by the barrier and on the change of car centre-of-gravity velocity were investigated.

Reference [16] presents experimental and numerical research of Suzuki Swift car impact at 45.5 km/h velocity, perpendicular to SP-04/2 barrier section without and with a foam-composite overlay. The cap consists of glass-fibre composite (one layer of plane weave fabric weighing 450 g/m<sup>2</sup>) with the trapezoidal outline and filled with polyurethane foam. The guiderail was attached to IPE140 posts fixed in the thick concrete slab. The following numerical and experimental quantities were compared: the time-history of the car centre-of-gravity acceleration, deformation of the vehicle and barrier, and the energy absorption.

Borkowski, et al. [2] investigated numerically the effect of the impact angle of the Suzuki Swift car on the concrete road barrier. The paper shows the motion trajectories and deformations of the vehicle, corresponding to the collision angles of 10°, 20°, 30°, 40°. The numerical car model was taken from the NCAC library. The next paper [3] develops

numerical modelling and simulation of the TB11 and TB32 crash tests taking into account fixed or movable segments of the concrete road barrier. The results include the behaviour and deformation of vehicles and the ASI index. The tests were performed using the Geo Metro (TB11) and the Chrysler Neon (TB32) FE models, collected from the NCAC library. Deformable connections and fittings were modelled using the 4-node shell finite elements.

A review of the patent databases shows various solutions modifying road barrier structures [1, 5-7, 14, 15, 20-24, 26, 27]. Patents and patent applications do not apply to barriers on road bends. Patents [5-7, 15, 20, 24, 27] propose various modifications of guide bar – post connectors. However, in these solutions, stability of guiderail during the impact may be lost. U.S. Patent [21] proposes a cover of the entire road barrier, including the posts and the bottom horizontal belt, in the form of an oval shell made of a deformable material (rubber-fabric), filled with foam in the guide surrounding, with tensioning connectors on the cover back. This solution is designed to protect motorcyclists.

Patent [23] presents a solution in the form of an energy-intensive corrugated element to replace a spacer between the guide and the post. This solution assumes that in the case of car collision with the barrier, the energy consuming element shortens plastically and absorbs the impact energy. However, this solution does not take into account potential loss of stability of the guiderail when too compliant plastic connectors between the posts and the guide bar are used. A similar solution is contained in Patent [14]. Patent application [1] proposes a device parallel to the guide, mounted under the guiderail to facilitate sliding of the car by introducing a set of vertical rollers and absorbing energy by means of a corrugated metal sheet. However, such a device would work correctly for a rigid concrete barrier, for example.

Patent [26] applies the reinforced thermoplastic composite coating, having thickness close to the guide thickness and the matched shape of the guide. The composite coating is joined to guide A by means of additional screws and screws connecting the posts and the guiderail, and the guide segments together. The author argues that the coating has large energy-intensive properties.

In patent application [22], trapezoidal or hemispherical energy-intensive multi-layer overlay to guide B of the road barrier is proposed. Cap segments are not interconnected.

The paper examines the SP-05/2 outer barrier of the N2-W4-A class (the producer: Stalprodukt JSC, Bochnia) with the B-type guide bar, located on a horizontal arch to an accelerated traffic main road (Polish code: GP), with the allowable radius of the road axis belonging to the range of 140–220 m. In order to ensure accepting the TB11 crash test, a rubber/foam/composite overlay has been designed, which was combined with the B guide with screw connectors using only the empty holes in the guide axis, at 2.00 m intervals. The overlay is flame retardant, resistant to weathering and required chemical effects, increases flexibility and strength of the barrier, reduces vehicle–barrier friction, and its estimated durability is 30 years.

The study develops a method for numerical modelling and simulation of the unmodified (a straight barrier) and modified (a barrier in a horizontal concave arch) TB11 crash test, without and with the overlay, including deformable joints with limited load capacity,

contact with friction, tire pressure, posts embedded in deformable subsoil, gravity load, damping, et al. The TB11 virtual crash tests have been conducted for the four above-mentioned barrier design systems.

## 2. Crash test indices

Standard [10] defines the criteria for crash tests and the test methods to which road restraint systems should be subjected. Standard [11] describes action classes in reference to protective road barriers via determining their functional characteristics, such as the restraint level, the working width, the collision intensity level. Standards [10, 11] do not include road bends.

The restraint levels are determined based on crash tests, and come in [2]: small T1, T2, T3; normal N1, N2; increased H1, H2, H3; very high H4a, H4b. In the case of N2 restraint level, acceptance of TB11 and TB32 crash tests is required (Table 1).

Table 1. TB11 and TB32 crash tests conditions [2]

Crash test	Impact velocity	Collision angle	Total car mass	Vehicle type
TB11	100 km/h	20°	900 kg	car
TB32	110 km/h	20°	1500 kg	car

The collision intensity level is a parameter reflecting the impact of collision on the vehicle occupants, measured by the acceleration severity index, ASI, and the theoretical head impact velocity, THIV. The ASI index is a dimensionless quantity calculated based on the time-histories of Cartesian components of the car centre-of-gravity acceleration, according to the complex algorithm given in Ref. [10]. The THIV velocity is calculated according to subsequent complex algorithm also given in Ref. [10]. The A level of the acceleration severity index corresponds to the conditions:  $ASI \leq 1.0$ ,  $THIV \leq 33$  km/h.

The working width is the distance between the side face of the barrier from the traffic side before the collision and the maximum dynamic lateral position of any greater part of barrier (Fig. 1). The working width is a measure of the barrier deformation. Standard [11] stands 8 levels of working width; in level W4, distance  $W \leq 1.3$  m. The barrier and the cap should preserve the integrity after collision with the vehicle.

The VCDI parameter is a deformation index of the vehicle compartment. The VCDI parameter record includes both the location and extent of damage to the car cab, in the form of XYabcdefg where XY – place of deformation (capital symbols), abcdefg – seven indices defining percent reduction in the seven characteristic interior dimensions of the cabin [11].

The car, after collision with the barrier and shifting in contact with the barrier, should bounce from the barrier so that the wheel traces do not exceed the line parallel to the barrier face original line, which is located at a distance of  $A = 2.2$  m + the car width + 16% of the car length (Fig. 2). In the case of a Suzuki Swift car, one obtains  $A = 4.4$  m. Not to exceed the line concerns the reflection field of length of  $B = 10$  m, measured from the exit point

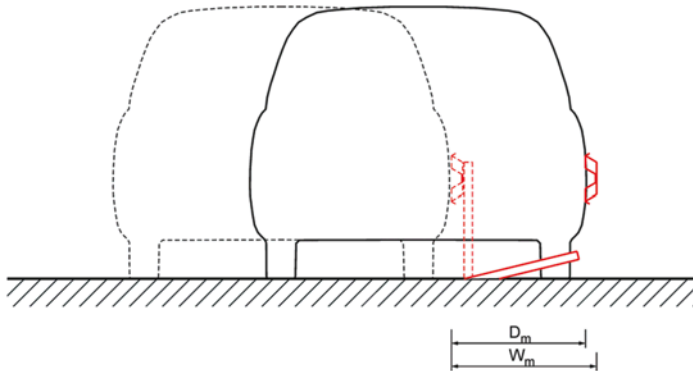


Fig. 1. Dynamic deflection,  $D_m$ , and working width,  $W_m$ , to example of barrier without spacer [11]

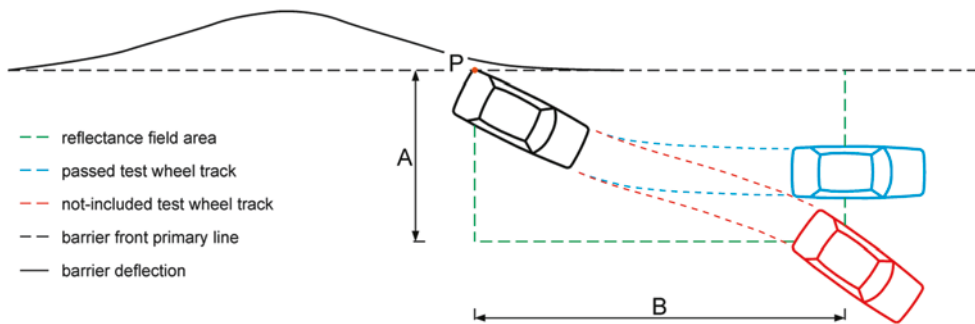


Fig. 2. Wheel trajectories of vehicle motion and reflection field [11]

of the last wheel beyond the barrier face original line. Locking the vehicle by the barrier, overturn or skidding of the vehicle are unacceptable.

The total weight of the vehicle also includes an ATD dummy (an anthropomorphic test device representing the 50<sup>th</sup> percentile of adult male), used in the TB11 experimental test to evaluate the occupant motion during the crash test.

### 3. Examined systems and simulated crash tests

The research object is the SP-05/2 road barrier of the N2-W4-A category. The barrier manufacturer (CE No. 1826-CPD-2.9.07-DR17) is Stalprodukt joint-stock company (JSC), Bochnia, Poland. The barrier is made from hot-dip galvanized S235JR steel. M16 bolts of strength class 4.6 are used in all connections. The barrier comprises a B-type guardrail, Sigma-100 posts with length of 1.90 m and spacing of 2.00 m. The TB11 crash test results announced by the barrier producer are as follows:

ASI = 0.8, W = 1.00m, THIV = 23km/h, VCDI = RF0001000.

Test sections of length of 60.00 m constitute a straight barrier (SB) and a curved barrier (CB) of radius of 150 m. This is the smallest radius of curvature of an outer barrier, which allows a traffic speed of 110 km/h. The barriers without (SB, CB) or with (SBC, CBC) the CFR2 covering system (described in next section) are under consideration. The simulated crash tests have the following codes: TB11/SB/20, TB11/SBC/20, TB11/CB/20, TB11/CBC/20. The intersection point of the car longitudinal axis with the guiderail axis (the vehicle impact point position) is set to 8.00 m before the centre of 60 m long barrier sections. A Geo Metro (Suzuki Swift) car, taken from the NCAC library [5], is used, which was under necessary modifications (see Section 6).

### 4. Description of CFR2 overlay

The flame retardant covering CFR2 [17] consists of glass-polyester composite segments partly fulfilled with polyurethane foam (Figs. 1, 2). The segments are connected to the B-type guide bar with M16/80 bolts of class 8.8, using thick rectangular rubber pads produced of 70°ShA EPDM rubber and rectangular dip galvanized steel washers of type A. The bolt joints are located in existing empty holes in the longitudinal axis of the guide bar. The covering is manufactured using hand lay-up technology. The CFR2 covering has a smooth front surface protected with gelcoat.

The continuous CFR2 covering system is composed of segments with a length of 4.70 m, overlapping one another in such a way that the effective length of each segment equals 4.00 m (Fig. 5). A cross-section of the overlay is correlated to the cross-section of the B-type guiderail including clearances needed to cover the barrier curvature, screw connectors, realization imperfections and thermal deformations. Technological fillet corners with a radius of 5 mm are used. The CFR2 overlay is composed of the GFRP composite front shell, the GFRP composite rear shell and the polyurethane foam core in two channels. A ply sequence in the front shell, with a total thickness of 4 mm, is as follows: gelcoat, CSM450 mat, two layers of WR600 [0/90] plain weave fabric, where direction 0 coincides the barrier axis. The back shell with a total thickness of 1.5 mm, closing the channels, is reinforced with one layer of CSM450 mat and protected with topcoat. The market glassware codes

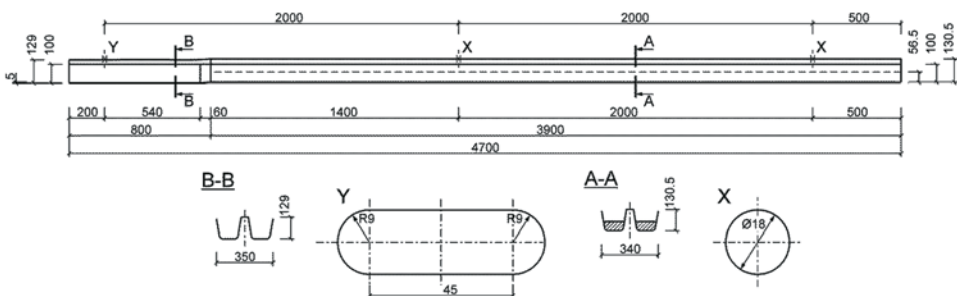
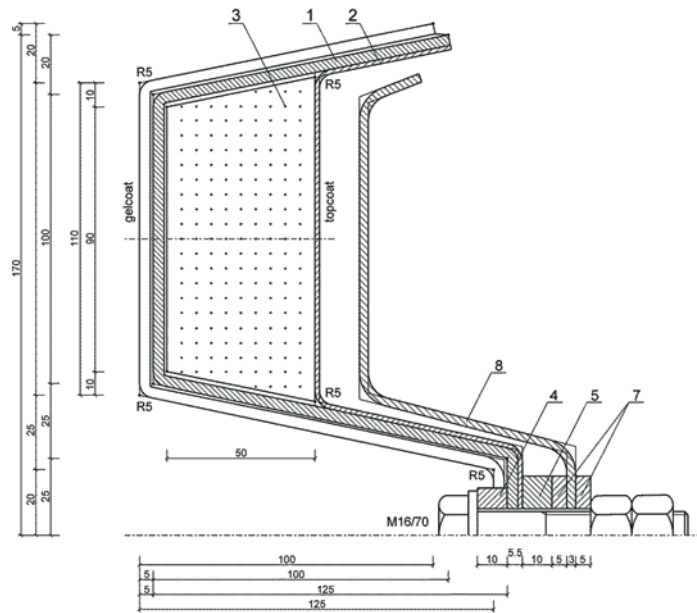


Fig. 3. Segment of CFR2 overlay



**Fig. 4. Cross-section of CFR2 overlay in node X axis: 1 – front laminate; 2 – rear laminate; 3 – polyurethane foam; 4 – front rubber pad; 5 – rear rubber pad; 6 – steel screw; 7 – rectangular dip galvanized pad of type A (manufacturer: Stalprodukt JSC, Bochnia); 8 – B-type guide bar**

comprise weight in  $g/m^2$ . The flame retardant polyester resin Polimal 104S (the producer: Organika-Sarzyna, Sarzyna, Poland) is used as the matrix. Polyurethane foam PUR S-42 of  $42 kg/m^3$  density is applied.

The CFR2 cap keeps B-type guiderail performance characteristics, including vehicle sliding on two overlay strips in appropriate height and the assembly of reflective elements in the channel in the cap axis. Graphical visualization of the SP-05/2 barrier with the overlay is shown in Figs. 6, 7.

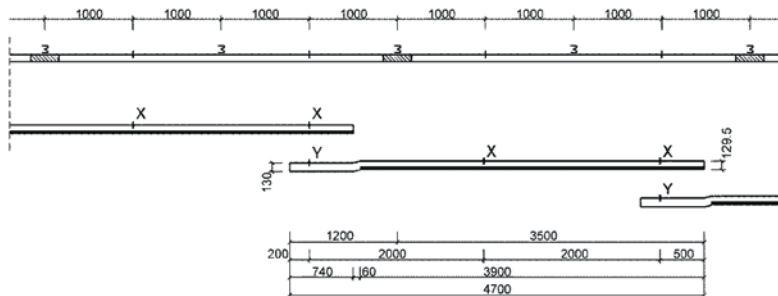
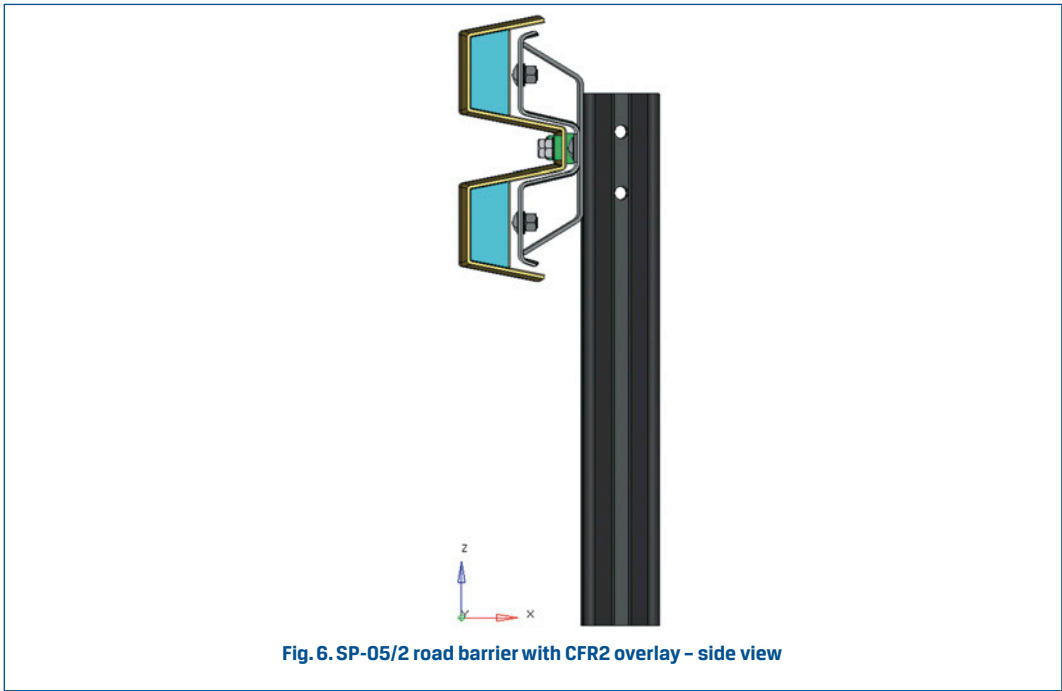
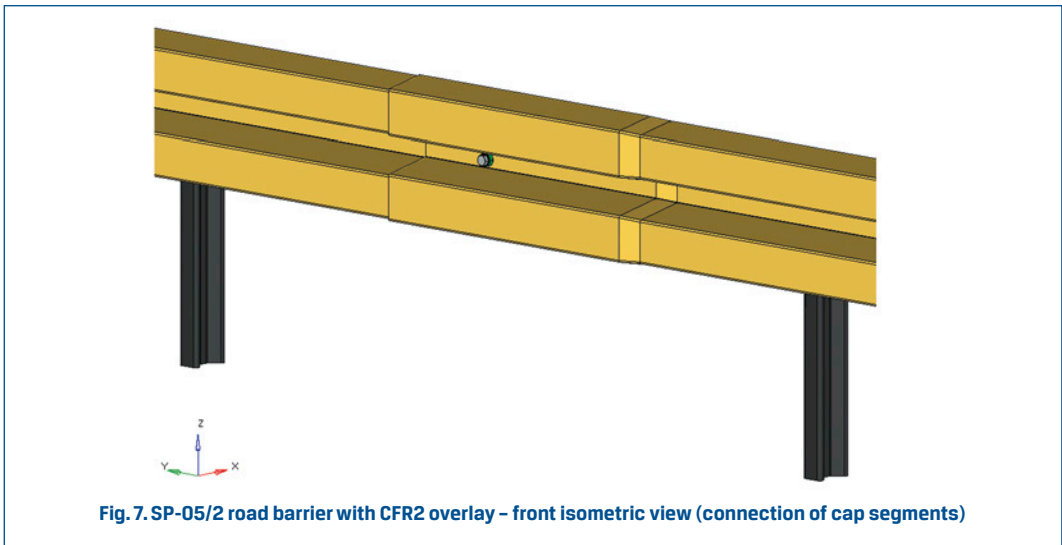


**Fig. 5. Connecting scheme of CFB2 overlay segments**



The principle of operation of the CFR2 overlay is as follows. After hitting the barrier by the vehicle at an angle of  $20^\circ$ , elastic deformation of the cap and rubber pads appears. The impact pulse is extended in time. The overlay is coming to the guide B, and based on it. It is followed by progressive destruction of cap main components, i.e., composite shells and foam core, but to the extent that maintains the integrity of the cap and the bolted



joints. The rubber pads soften the collision process. Friction between the vehicle and the gelcoat layer covering the cap is significantly reduced compared with the steel guide, which facilitates easier sliding of the vehicle on the barrier with the cap and contributes to securing the vehicle before skidding.

### 5. Material models of system parts

In order to describe material models and numerical modelling in subsequent parts, the original terms and symbols, used in manuals [12, 13] of the LS-Dyna system, are applied.

S235JR steel used to manufacture barrier parts have material constants taken from the data sheet [29]. Elastoplastic properties with isotropic hardening of steel are reflected by the \*MAT\_PIECEWISE\_LINEAR\_PLASTICITY (\*MAT\_024) model. Steel failure is defined by ultimate effective plastic deformation. Table 2 lists the values of material constants of S235JR steel. The tangent modulus value and the ultimate plastic deformation are taken from Ref. [19].

Table 2. Material constants of S235JR steel

Constant*	Value	Unit*	Constant name
RO	7.850×10 <sup>-9</sup>	t/mm <sup>3</sup>	material density
E	210000	MPa	Young's modulus
PR	0.3	-	Poisson's ratio
SIGY	372	MPa	yield strength
ETAN	1000	MPa	tangent modulus
FAIL	0.5	-	ultimate plastic strain (erosion)

\* Applied labels and units used in the LS-Dyna system.

A GFRP laminate reinforced with selected mat and fabric is modelled as a viscoelastic-brittle material using \*MAT\_ENHANCED\_COMPOSITE\_DAMAGE (\*MAT\_054) material model. This model is addressed to unidirectionally reinforced composites first of all, thus it only approximates the behaviour of composites occurring in the CFR2 covering. This model takes into account the Chang-Chang failure criterion [13]. The material constants of homogeneous laminas reinforced with CSM450 mat and WR600 fabric, the authors have identified experimentally in the Laboratory of Materials and Structures, Department of Mechanics and Applied Computer Science, Faculty of Mechanical Engineering, Military University of Technology, Warsaw, Poland, at room temperature, according to respective standards. The materials constants of laminas are collected in Table 3, with X – warp direction, Y – weft direction, Z – thickness direction.

PUR S-42 polyurethane foam is reflected by the \* MAT\_HONEYCOMB (\* MAT\_026) material model. It is used to model sandwich cores and anisotropic foams. The material constants (Table 4) and the shear stress vs. the volumetric strain and the normal stress vs. the volumetric strain curves are taken from Ref. [9].

The subsoil, in which Sigma-100 posts are embedded, is reflected by the \*MAT\_SOIL\_AND\_FOAM (\*MAT\_005) model. This is a simple model used to foams and subsoil in a case where the material constants are not fully defined. The material constants of the subsoil, given in Table 5, are taken from the National Crash Analysis Center (NCAC) website [31]. The asphalt pavement and the shoulder are modelled as non-deformable surfaces. Friction coefficients amount to 0.90 for the dry asphalt/concrete – tire pair and 0.68 for the dry hardened ground – tire pair [30].

**Table 3. Material constants of laminas**

No.	LS-Dyna Symbol	Value		Unit	Constant name
		CSM450	WR600		
1	RO	1.420×10 <sup>-9</sup>	1.680×10 <sup>-9</sup>	t/mm <sup>3</sup>	material density
2	EA	7060	15300	MPa	Young's modulus in fibre direction
3	EB	7060	15300	MPa	Young's modulus in matrix direction
4	PRBA	0.386	0.140	-	Poisson's ratio in laminate plane
5	GAB	2080	1770	MPa	shear modulus in laminate plane
6	GBC	2000	2000	MPa	shear modulus in YZ plane
7	GCA	2000	2000	MPa	shear modulus in XZ plane
8	YAFAC	2	2	-	weakening of compressive strength of fibres after matrix destruction by compression
9	DFAILT	0.02	0.02	-	ultimate strains at fibre tension
10	DFAILC	-0.02	-0.02	-	ultimate strains at fibre compression
11	EFS	0.05	0.05	-	effective ultimate strains
12	XC	216	197	MPa	compressive strength in fibre direction
13	XT	95.6	269	MPa	tensile strength in fibre direction
14	YC	216	197	MPa	compressive strength in matrix direction
15	YT	95.6	269	MPa	tensile strength in matrix direction
16	SC	45.5	34.8	MPa	shear strength in laminate plane

## 6. Numerical model of car used in TB11 tests

In virtual crash tests, the FE numerical model of Geo Metro (Suzuki Swift) car, developed by the NCAC (2013), is used

(Fig. 8). The vehicle suspension is viscoelastic. The vehicle numerical model includes more than 200 material models assigned to particular parts of car. Among them, the following main models can be distinguished: \*MAT\_ELASTIC (\*MAT\_001), \*MAT\_RIGID (\*MAT\_020), MAT\_PIECEWISE\_LINEAR\_PLASTICITY (\*MAT\_024), MAT\_LINEAR\_ELASTIC\_DISCRETE\_BEAM (\*MAT\_066).

Based on preliminary numerical tests, there were established the necessary changes in the car model impacting at an angle of 20° into the barrier, including:

- 1) changing tire model from \*AIRBAG model into \*AIRBAG\_SIMPLE\_PRESSURE\_VOLUME model,
- 2) declaration of tire pressure equal to 2.3 bar,
- 3) correction of suspension (application of MAT\_66 material model and BEAM elements in ELFORM\_6 formulation, stiffness and damping suspension adjustment, adding preload in dynamic relaxation process),
- 4) introduction of dynamic relaxation (influence of gravity forces) before starting vehicle collision with barrier,
- 5) declaration of linear velocity of vehicle and angular velocity of wheels at start time,
- 6) adjustment of wheel alignment and wheel rotation axis,
- 7) correction of contact options,
- 8) correction of control cards,
- 9) hourglass control (elimination of non-physical forms of vibration),
- 10) placing ELEMENT\_SEATBELT\_ACCELEROMETER at car centre-of-gravity on rigid solid element connected to chassis by means of \*CONSTRAINED\_EXTRA\_NODES bonds,
- 11) correction of stiffness of bonds.

The numerical model of the car consists of ~33500 finite elements.

**Table 4. Material constants of PUR S-42 polyurethane foam**

No.	Symbol	Value	Unit	Constant name
1	RO	$4.400 \times 10^{-11}$	t/mm <sup>3</sup>	material density
2	E	100	MPa	Young's modulus of fully compressed foam
3	PR	0.3	-	Poisson's ratio of fully compressed foam
4	SIGY	50	MPa	yield strength of fully compressed foam
5	VF	0.1	-	relative volume of fully compressed foam
6	EAAU EBBU ECCU	0.5	-	Young's modulus of uncompressed foam in directions A, B, C
7	GABU GBCU GCAU	1.0	MPa	shear modulus of uncompressed foam in directions A, B, C

**Table 5. Material constants of subsoil**

No.	Symbol	Value	Unit	Constant name
1	RO	$1.700 \times 10^{-9}$	t/mm <sup>3</sup>	material density
2	G	49.5	MPa	shear modulus
3	K	185	MPa	bulk modulus
4	AO	$1.213 \times 10^{-2}$	N <sup>2</sup> /mm <sup>4</sup>	plasticity function constant
5	PC	$-1.724 \times 10^{-1}$	MPa	ultimate tensile pressure

## 7. Numerical modelling of system parts

Parts of the SP-05/2 barrier section of length of 60 m are modelled using four-node shell finite elements in the Belytshko-Tsay formulation, with one integration point in the element plane (ELFORM 2) and five integration points through the thickness. The correction factor of transverse shear stresses is assumed equal to the theoretical value (SHRF = 0.8333).

The subsoil is reflected by cylinders (one cylinder per post) with a radius of 1.00 m and a height of 1.30 m, using solid elements in ELFORM1 formulation (constant stress solid element). In addition, the ground component is assigned to the Flanagan-Belytshko hourglass stiffness form (IHQ=4, QM=0.03). From the top, the soil has been closed with coating discretised with shell elements having a thickness of 1 mm and assigned properties of the \*\_MAT\_NULL (\*MAT\_009) material.

The \*CONTACT\_AUTOMATIC\_SINGLE\_SURFACE has been defined between each post and the shell closing the subsoil, taking into account dry friction with the friction coefficient FS=0.30. In addition, for the ground cylinders in the 16 m long impact zone the \*CONTACT\_INTERIOR is defined in order to correct their work at high distortion [13]. The safety barrier and the subsoil exhibit viscous damping properties in the stiffness formulation (\*DAMPING\_PART\_STIFFNESS), with damping ratios COEF=0.03 for steel and COEF=0.10 for subsoil.



**Fig. 8. Geo Metro car model - isometric view from top [31]**

The post/bracket/guide/pad screw connection is modelled with \*CONSTRAINED\_GENERALIZED\_WELD\_SPOT. The element card specifies the limit axial force  $S_n = 40200$  N and limit shear force  $S_s = 23316$  N, at which the connection is broken, according to the formula [28]:

$$\frac{\max F_n}{S_n} + \frac{|F_s|}{S_s} \geq 1,$$

where  $F_n, F_s$  – axial force and shear force in connection, respectively.

Modelling deformable bolted joints of the guiderail segments with each other and with the

CFR2 overlay, used in the SP-05/2 barrier, is presented in Ref. [18]. Each screw connection of guide segments with each other is mapped by means of elastic-damping elements and used in the shell model of guide bar.

Screw connections of guide segments with the CFR2 overlay are mapped by means of \*CONSTRAINED\_GENERALIZED\_WELD\_SPOT elements because the composite coating is destroyed first. Modelling in this way allows simulation of potential breaking of bolted joints during collision with the vehicle.

Figures 9–12 present the numerical model of the barrier in curve, without and with the CFR2 covering.

For all pairs of the barrier components (guardrail, posts, brackets, rectangular washers) contact model \*CONTACT\_AUTOMATIC\_SINGLE\_SURFACE was defined taking into account the Coulomb dry friction (friction coefficient  $FS=0.25$ ).

Laminates in the CFR2 overlay are modelled using four-node shell elements in the Belytshko-Tsay formulation, with one in-plane integration point (ELFORM 2) (Figs. 11, 12). Polyurethane foam is modelled using solid elements with ELFORM1 formulation and the Flanagan-Belytshko hourglass stiffness form (IHQ=4, QM=0.05) (Fig. 12). The covering exhibits the stiffness viscous damping (\*DAMPING\_PART\_STIFFNESS), with damping ratios  $COEF=0.10$  for GFRP laminates and  $COEF=0.15$  for PUR S-42 foam [12, 13].

Contact between all possible pairs of the covering and barrier components was defined using the \*CONTACT\_AUTOMATIC\_SINGLE\_SURFACE model and respective kinematic friction coefficients, i.e.,  $FS=0.14$  between laminates and steel elements,  $FS=0.26$  between foam and steel elements,  $FS=0.30$  between foam and laminates.

Values of friction coefficients have been identified from experiments performed in the Tribological Tests Laboratory, Department of Advanced Materials and Technologies, Faculty of Materials Engineering, Military University of Technology, Warsaw, Poland.

The numerical model of barrier/covering/subsoil system consists of ~158000 finite elements.

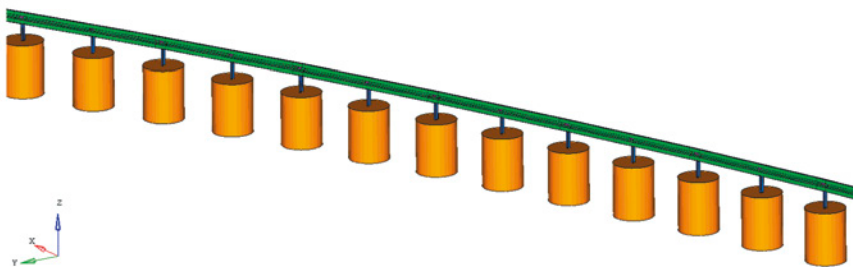


**Fig. 9. Visualization of curved section of SP-05/2 barrier - isometric view**

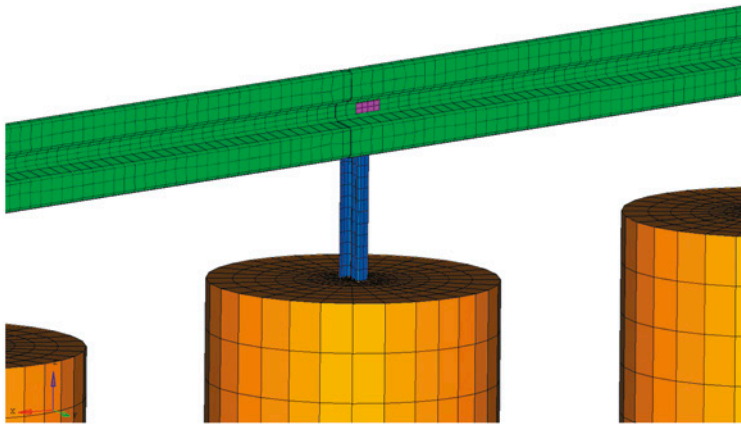


Fig. 10. Discretization of SP-05/2 barrier and subsoil - front isometric view

## 8. Simulation of crash tests

The simulation results of virtual crash tests considered in this study are illustrated in Figs. 13–21. Positions of the moving car and the barrier at selected time points are shown in Figs. 13-18, respectively in reference to TB11/SB/20 (Fig. 13), TB11/SBC/20 (Fig. 14), TB11/CB/20 (Figs. 15, 16) and TB11/CBC/20 (Figs. 17, 18). Figures 15 and 16 can show unacceptable vehicle skidding.

Figure 19 compares the energy balance diagrams in reference to TB11/CB/20 and TB11/CBC/20 crash tests, i.e., performed for the curved barrier without and with the CFR2 covering. These charts are used to control accuracy of modelling and simulation, as well as to assess redistribution of the kinetic energy, the internal energy, and the friction, as a result of application of the CFR2 covering. The hourglass energy should not exceed 5% of the total energy. Figures 20, 21 compare time histories of the ASI index for the straight barrier without and with the CFR2 covering (Fig. 20) and for the curved barrier without and with the CFR2 covering (Fig. 21). Table 6 compares four performed virtual crash tests, both quantitatively and qualitatively, including ASI, THIV, W, VCDI parameters and occurrence of car skidding.

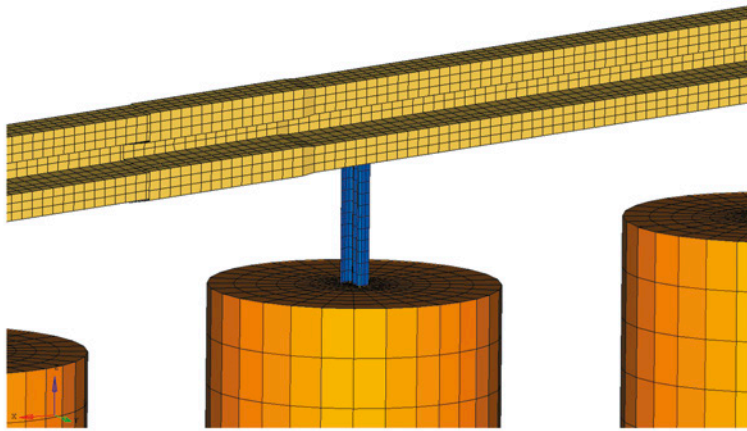


Fig. 11. FEM model section of SP-05/2 barrier with CFR2 overlay – front isometric view

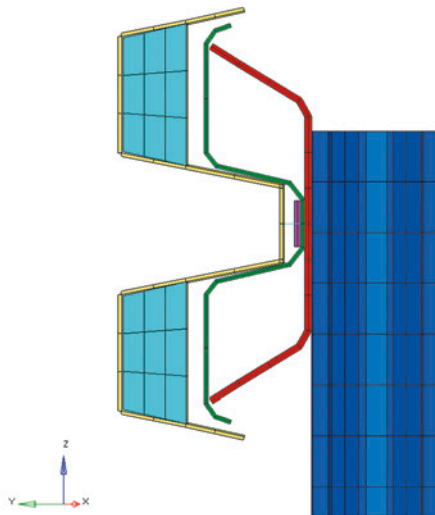


Fig. 12. FEM mesh of polyurethane foam and visualization of thickness of shell elements with offset - side view

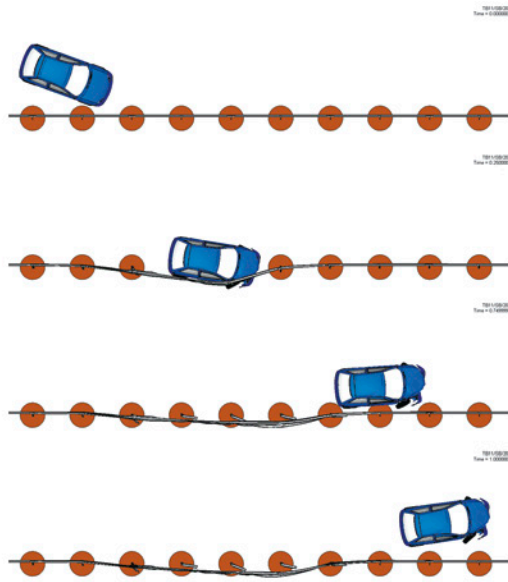


Fig. 13. Animation of TB11/SB/20 crash test – top view

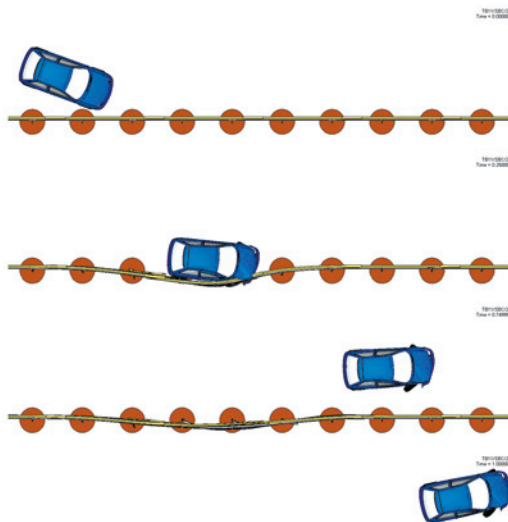


Fig. 14. Animation of TB11/SBC/20 crash test – top view

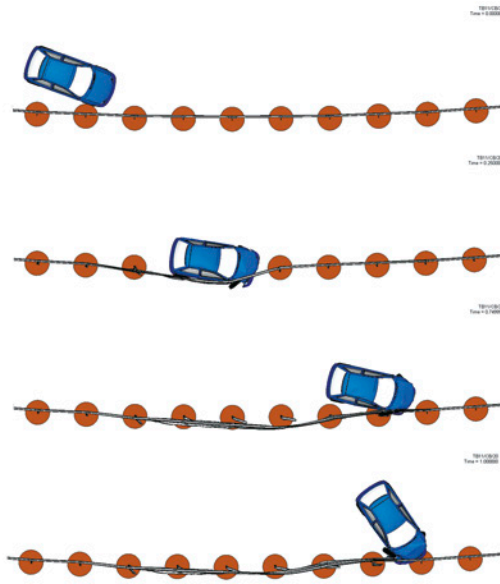


Fig. 15. Animation of TB11/CB/20 crash test - top view

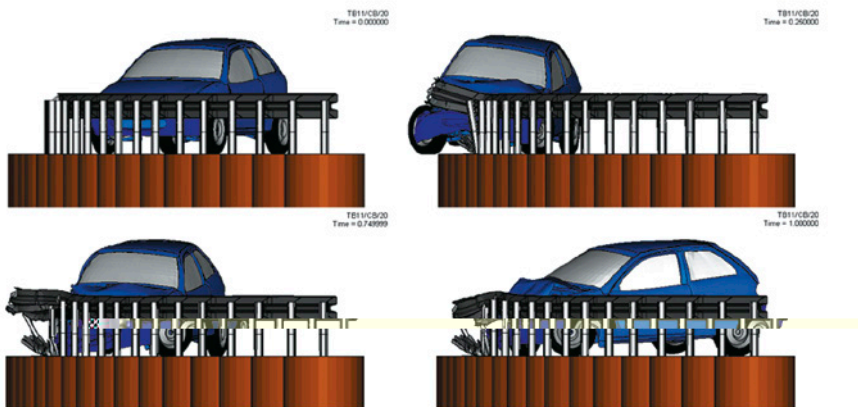


Fig. 16. Animation of TB11/CB/20 crash test - front view

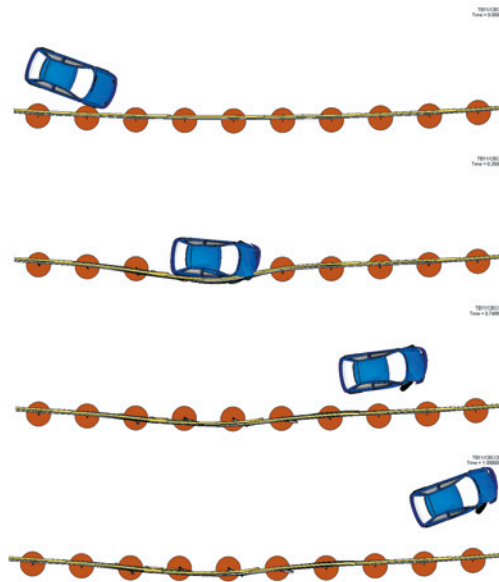


Fig. 17. Animation of TB11/CBC/20 crash test - top view

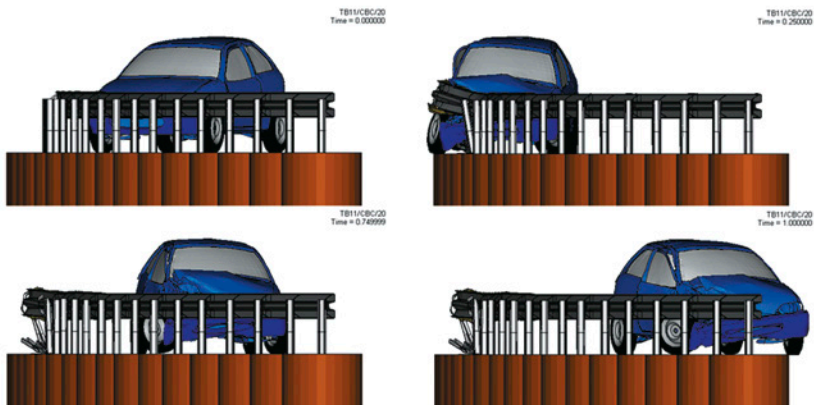
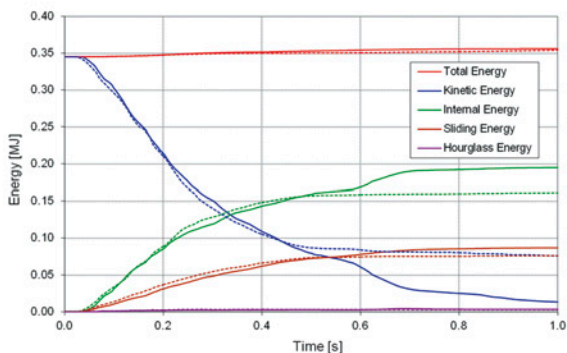
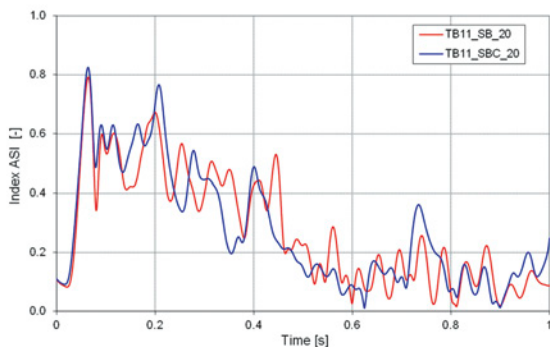


Fig. 18. Animation of TB11/CBC/20 crash test - front view



**Fig. 19. Comparison of energy balances for testing vehicle collision with barrier in arc: TB11/CB/20 – solid lines; TB11/CBC/20 – dashed lines**



**Fig. 20. Comparison of ASI index time histories for TB11/SB/20 (red curve) and TB11/SBC/20 (blue curve) tests**

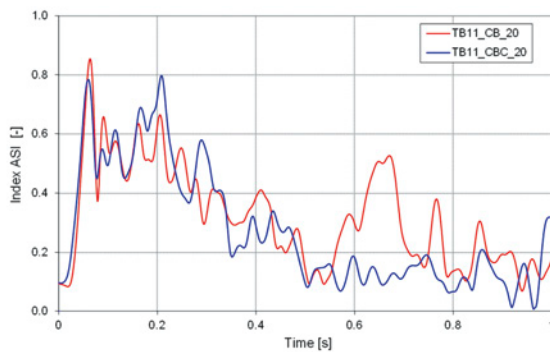


**Fig. 21. Comparison of ASI index time histories for TB11/CB/20 (red curve) and TB11/CBC/20 (blue curve) tests**

**Table 6. Quantitative and qualitative comparison of virtual TB11 crash tests**

Crash test	ASI [-]	THIV [km/h]	W [m]	VCDI	Car skidding
TB11/SB/20	0.8 (0.79)	19 (18.90)	0.9 (0.87)	RF0010000	no
TB11/SBC/20	0.8 (0.82)	21 (20.96)	0.8 (0.77)	RF0010000	no
TB11/CB/20	0.9 (0.85)	21 (20.91)	0.8 (0.81)	RF0010000	yes
TB11/CBC/20	0.8 (0.80)	19 (19.21)	0.7 (0.72)	RF0010110	no

Based on the simulations presented in this study, the following main conclusions are formulated:

- 1) The impact of the CFR2 covering on the course of the TB11 crash test for a straight barrier is small. Repulse of the car from the modified barrier is slightly increased, but handling of the vehicle is higher due to the increased damaging of the front wheelset in the case of the unmodified barrier (Figs. 13, 14). The ASI index value is nearly the same in both cases (Fig. 20).
- 2) The impact of the CFR2 covering on the course of the TB11 crash test for the barrier in a horizontal concave arc of a radius of 150 m is significant (Figs. 15–18, Table 6). In the case of the unmodified barrier, there is an unacceptable skidding of the vehicle (Figs. 15, 16). In the first phase of the modified barrier test (time less than 0.45s), there occurs a marginal reduction in the kinetic energy and a slight increase of the internal energy and friction compared with the unmodified barrier (Fig. 19). In further part of the modified barrier test, the kinetic energy, internal energy and friction remain at a constant level, ensuring accepting the crash test (Fig. 19). The exact value of the ASI index is lower by 6.5% compared to the unmodified curved barrier (Fig. 21). The motion trajectory and controllability of the vehicle are much better for the modified curved barrier (Figs. 17, 18).
- 3) The curvature of the unmodified SP-05/2 road barrier increases the absorbed energy significantly and causes the car skidding (Fig. 19). The CFR2 covering system assembled with the curved barrier eliminates car skidding as well as front wheel set failure, and improves handling of the vehicle after the collision.

## 9. Conclusions

The study develops numerical modelling and simulation of car–road barrier impact tests. The numerical modelling and simulation methodology is based on:

- advanced material models with failure of barrier and covering components, bolt connections, subsoil, and a car;
- tire pressure, contact with friction, gravitational load, possible erosion of finite elements, hourglass control;
- posts embedded in deformable solid subsoil;
- shell FE modelling of rectilinear and curved barriers;

- physical modification of Geo Metro FE model taken from NCAC public library;
- reliable values of friction coefficients based on the authors' experiments and appropriate references;
- viscous damping of selected components of the system (barrier, covering, subsoil).

The TB11 virtual crash tests were conducted for the SP-05/2 barrier of the N2-W4-A category, in four cases, i.e. for the unmodified barrier / barrier equipped with CFR2 covering, located on the straight road / road bend of radius of 140 m. Effects of the barrier curvature and the covering equipment on the course of the TB11 crash tests were investigated. It has been pointed out that the CFR2 covering system assembled with the SP-05/2 road barrier in an arc of radius of 150 m eliminates car skidding and front wheel set failure, and improves handling of the vehicle.

Design of overlays on guides of curved road barriers is a complex issue because it requires simultaneous fulfilment of following design conditions:

- 1) an overlay cannot be too energy-intensive, as it will absorb too much kinetic energy, making it impossible to move the vehicle on the road;
- 2) an overlay cannot be too rigid, as it will induce too large repulse of vehicle on the road;
- 3) an overlay cannot be too weak in terms of strength, because of collapse during collision;
- 4) screw connections of an overlay with the guide must ensure the integrity of the restraining system during collision with a vehicle;
- 5) the shape of overlay must provide performance features of the B-type steel guide;
- 6) the geometric-material parameters of an overlay must be chosen so that a cap is not part of the gauge road and provide acceptance of crash test.

The CFR2 rubber/foam/composite overlay to the guide B of an outer road barrier of the N2-W4-A category, with the posts spaced 2.00 m, applied to bands of accelerated traffic main roads, with a radius of 140–220 m, increases – in suitable proportions – flexibility, energy consumption, and strength of barrier. In the case of vehicle collision with the barrier according to the TB11 test, the CFR2 overlay allows for the conditions imposed on the collision parameters. The CFR2 cap is fully compatible with currently exploited class of road safety barriers of the N2-W4-A category, with B-type guides, inter alia, the SP-05/2 barrier, which reduces the cost of its implementation. Quick installation with screw connectors, using only free holes in the guide, does not cause traffic delays.

## Acknowledgments

The study was supported by the National Centre for Research and Development, Poland, as a part of the research project PBS1/B6/14/2012 (acronym ENERBAR), realized in the period 2013-2015. This support is gratefully acknowledged. The authors express their thanks to Pawel Dziewulski, Ph.D. (Military University of Technology) for consultation in the field of modelling and to Cezary Senderowski, Ph.D. (Military University of Technology) for performing the experimental friction tests.

## References

- [1] Alvarez M.: *Crash barrier protection element and crash barrier incorporating said protection element*, Patent application EP2426259A1, 2012-03-7.
- [2] Borkowski W., Hryciów Z., Rybak P., Wysocki J.: *Testing the results of a passenger vehicle collision with a rigid barrier*, J. Kones: Powertrain and Transport, 17, 1, 2010.
- [3] Borkowski W., Hryciów Z., Rybak P., Wysocki J.: *Numerical simulation of the standard TB11 and TB32 tests for a concrete safety barrier*, J. Kones: Powertrain and Transport, 17, 4, 2010.
- [4] Borovinsek M., Vesenjank M., Ulbin M., Ren Z.: *Simulation of Crash Tests for High Containment Levels of Road Safety Barriers*, Engineering Failure Analysis 14 (2007) 1711–1718.
- [5] Bowyer S.: *Road safety barrier*, Patent US2007116513, 2007-05-24.
- [6] Conway S.J., Mauer F., Dallas J.: *Roadway Guardrail System*, Patent CA2697037, 2009-02-26.
- [7] Cucchiatti M.: *Reinforced roadside barrier*, Patent EP1832681, 2007-09-12.
- [8] Dziewulski P.: *Numerical analysis of car - road barrier crash tests* [in Polish], Proc. III Symp. on Advances in Manufacturing Technologies and Machinery Structures, Kazimierz Dolny, Poland, pp. 43-49, 2009.
- [9] Dziewulski P.: *Badanie wybranych struktur do poprawy energochłonności drogowych barier ochronnych*, Praca doktorska, Wydział Mechaniczny, Wojskowa Akademia Techniczna, Warszawa, 2010.
- [10] EN 1317-1:2010. *Road restraint systems – Part 1: Terminology and general criteria for test methods*.
- [11] EN 1317-2:2010. *Road restraint systems – Part 2: Performance classes, impact tests acceptance criteria and test methods for safety barriers including vehicle parapets*.
- [12] Hallquist J. O.: *LS-DYNA Keyword User's Manual*, Livermore Software Technology Corporation, May 2007.
- [13] Hallquist H. J. O.: *LS-DYNA Theory Manual*, Livermore Software Technology Corporation, USA, March 2006.
- [14] Holecz F.: *Barriera protettiva dei margini autostradali e della zona spartitraffico*, Patent 432573, Switzerland, 20-08-1966.
- [15] Impero P.: *Road Safety Barrier*, Patent W02009090681, 2009-07-23.
- [16] Kiczko A., Niezgoda T., Nowak J., Dziewulski P.: *Numerical implementation of car impact into the modified road barrier*, J. Kones: Powertrain and Transport, 17, 3, 2010, pp. 189-196.
- [17] Klasztorny M., Niezgoda T., Romanowski R., Nycz D., Rudnik D., Zielonka K.: *Nakładka na prowadnicę bariery ochronnej na łuku drogi*, Zgłoszenie patentowe UP RP, 6.10.2014.
- [18] Klasztorny M., Kiczko A., Nycz D.: *Modelowanie numeryczne i symulacja rozciągania połączenia śrubowego segmentów prowadnicy B bariery drogowej*, 13. Konferencja Naukowo-Techniczna nt. Techniki Komputerowe w Inżynierii, Licheń Stary, 6–9 maja 2014, Materiały Konferencji, s. 77-78.
- [19] Kossakowski P.G.: *Simulation of Ductile Fracture of S235JR Steel Using Computational Cells with Microstructurally-Based Length Scales*, Journal of Theoretical and Applied Mechanics 50, 2, 2012, pp. 589-607.
- [20] Kwan C.H.: *Shock absorber for road safety barrier*, Patent AU2006235944, 2006-11-10.
- [21] Masinelli G., Piastra R.: *Method for making a protective device for guiderrails, and a protective de-vice for guiderrails*, Patent US7257875 B2, 2009-03-26.
- [22] Niezgoda T., Barnat W., Dziewulski P., Sławiński G., Kędziński P.: *Smart panel*, Zgłoszenie patentowe PL 403165, 2013-03-15.
- [23] Patent 76P29467P.L00. *Urządzenie pochłaniające energię zderzenia oraz zespół ochronny drogowy lub pojazdu zawierający co najmniej jedno urządzenie pochłaniające energię zderzenia*.
- [24] Rafferty J., Wallace H., Colquhoun T.: *Barrier Construction, Joining And Orientation System*, Patent W02009021290, 2009-02-19.
- [25] Ren Z., Vesenjank M.: *Computational and Experimental Crash Analysis of the Road Safety Barrier*, Engineering Failure Analysis 12 (2005) 963–973.
- [26] Tang J.: *Wave-shaped guiderail panel*, Patent WO 2013/107203 A1, 2012-10-30.
- [27] Wallace H., Colquhoun T., Hare H.J., Whiteside M.: *Improved Road Barrier*, Patent W02010105307, 2010-09-23.
- [28] [http://metale.pwr.wroc.pl/files/A.Biegus-Polaczenia\\_Srubowe.pdf](http://metale.pwr.wroc.pl/files/A.Biegus-Polaczenia_Srubowe.pdf). Biegus A.: *Projektowanie konstrukcji stalowych według Eurokodu 3; Część 4 - połączenia śrubowe*; Materiały dydaktyczne, 07.04.2013.
- [29] <http://www.salzgitter-mannesmann.pl/>. *Systems, Service, Steel*, Salzgitter, January 7, 2013.
- [30] <http://hpwizard.com/tire-friction-coefficient.html>. *Tire friction and rolling resistance coefficients*, TA-Technix Coilover Kits, Denmark, January 7, 2013.
- [31] <http://www.ncac.gwu.edu/vml/models.html>. *Vehicle Models*, National Crash Analysis Center, USA, January 7, 2013.